Synergistic interplay of Zn and Rh-Cr promoters on Ga_2O_3 based photocatalysts for water splitting

Marta Borges Ordoño,[a] Shunsaku Yasumura,[a] Pieter Glatzel,[b] and Atsushi Urakawa*[a]

Photocatalytic water splitting activity of a wide-bandgap material, Ga_2O_3, is greatly boosted with the addition of Zn and Rh-Cr co-catalyst at optimum loadings. To date, however, the exact roles of the co-catalysts and particularly the origin of their synergistic functions are not clarified. Herein, we present how the optimum Zn loading on Ga_2O_3 leads to creation of $ZnGa_2O_4/Ga_2O_3$ heterojunction favorable for charge separation through the information on the occupied and unoccupied electronic states of Zn and Ga elucidated by X-ray absorption and emission spectroscopic methods. The function of Rh-Cr as electron sink and reduction site was proven by photocatalytic experiments using an electron scavanger (Ag^+) and by learning where Ag deposites and its effects on the photocatalytic activity. Finally, perturbation of Zn electronic structure by photo activation was evidenced by modulation exciatation X-ray absorption spectroscopy. Importantly, Rh-Cr markedly enhanced the level of the perturbation, serving as a proof of direct communication and synergy between the electronic states of Zn, present in $ZnGa_2O_4$, and Rh-Cr deposited on Ga_2O_3.

Introduction

Photocatalytic water splitting has been extensively studied over the past years as a sustainable path to harvest sunlight to convert the energy contained in photons into the form of chemical energy such as hydrogen.[1-3] TiO_2 is the most widely investigated photocatalyst material because of its abundance, non-toxicity, and low cost;[4] however, the low H_2 productivity achieved by TiO_2 has motivated researchers to look for alternative semiconductor materials.[5-7] Among them, Ga_2O_3 exhibits excellent activity for pure water splitting under UV-light due to its wide bandgap (4.6 eV) sufficient for the formation of hydrogen as well as oxygen.[8] Nevertheless, bare metal oxides generally lack surface sites to efficiently activate the redox reactions and often show poor photocatalytic water splitting performance. The most common strategy to improve the catalytic activity is the introduction of co-catalyst(s) to promote electron trapping ability near the catalyst surface, extending the life-time of electrons and holes generated upon light excitation and facilitating the redox reactions of adsorbed species at surface active sites of or near the co-catalyst.[9] Noble metals such as Pt, Ru, and Rh,[8] and combinations of metal oxides such as NiO,[10] RuO_2,[11] and $Rh_{2-y}Cr_yO_3$ (or simple written as Rh-Cr)[12] are commonly reported as effective co-catalysts when optimally loaded on the photocatalysts. Particularly for Ga-based oxide materials, rhodium and chromium mixed oxide was found greatly beneficial for overall water splitting as demonstrated for the visible-light active $(Ga_{1-x}Zn_x)(N_{1-x}O_x)$ material.[11,13] More recently, $Rh_{2-y}Cr_yO_3$ deposited on Zn-doped Ga_2O_3 was found to exhibit one of the highest water splitting activity reported to date (21.0 mmol of H_2 h^{-1} and 10.5 mmol O_2 h^{-1}) under UV-light irradiation.[14,15]

Promotion of photocatalytic functions by co-catalyst(s) generally involves the formation of additional energy states which facilitate charge carriers (electron-hole) separation by electron trap or donation from the co-catalyst to the semiconductor material.[16] For the most active Rh-Cr and Zn co-doped Ga_2O_3 material, the function of Rh-Cr is generally explained as an electron sink whereas the role of Zn is not clear,[17] although we have recently shown that the recombination of charges is greatly delayed by Zn promotion, thus enhancing the life-time of active redox sites and consequently the photocatalytic activity.[18] However, the origin of the promotional effects and detailed insights into the electronic structure of the materials, particularly the synergistic functions of Rh-Cr and Zn co-promotion at an optimum loading of co-catalysts (especially Zn),[14, 17] are not known. Since the unique combination of the constituting elements of Rh-Cr/Zn-Ga_2O_3 catalyst affords outstanding photocatalytic performance in pure water splitting by a few orders of magnitude higher than those generally reported,[14, 18] it is imperative to precisely understand the promotional and synergistic effects of Rh-Cr and Zn towards the rational photocatalyst design for hydrogen production from water with sunlight.

Reflecting this background, herein we uncovered the effects of Zn and Rh-Cr promotion through understanding their impacts on the electronic structure of Ga_2O_3-based photocatalysts. Element selective X-ray absorption and emission spectroscopies (XAS and XES) were employed to learn about the structures of unoccupied (related to conduction band) and occupied (related to valance band) electronic states of Zn and Ga within the catalyst materials, respectively.[19-21] In contrast to the integral information expressed as bandgap commonly gained measured by UV-Vis diffuse reflectance spectroscopy (UV-Vis DRS),[22, 23] the information from XAS-XES uniquely shows how the electronic structures of atoms in a material are altered[24] and, together with additional structural insights gained by electron microscopy and X-ray diffraction, the exact functions of Zn-Ga

heterojunction favourable for charge separation could be elucidated. On the other hand, the function of Rh-Cr as reduction and H_2-evolution site was verified by a control experiment using Ag^+ as electron scavenger as well as by monitoring the change in the electronic structure of Cr by XAS. Finally, the direct involvement of Rh-Cr component on the charge separation in Zn element was evidenced by means of XAS combined with a modulation excitation technique,[25] firmly explaining the electronic interactions of the two promoters and their concerted synergistic functions resulting in the drastic boost of the photocatalytic water splitting activity of Ga_2O_3.

Experimental section

Photocatalysts preparation

Zn-modified Ga_2O_3 catalysts were prepared by the impregnation method followed by a thermal treatment. First, β-Ga_2O_3 (≥99.99% trace metal basis, Sigma-Aldrich) raw material was calcined at 773 K for 3 h. The β-Ga_2O_3 powder was then impregnated with an aqueous solution of $Zn(NO_3)_2 \cdot 6H_2O$ (99.999% trace metal basis, Sigma-Aldrich) and calcined at 1123 K for 6 h, the Zn loading was varied from 0 to 70 wt% (based on the weight of Zn with respect to that of Ga_2O_3). Zn-modified Ga_2O_3 was then impregnated with Rh (0.5 wt%) and Cr (0.75 wt%) w.r.t Zn-Ga_2O_3 with an aqueous solution containing $RhCl_3$ and $Cr(NO_3)_3 \cdot 9H_2O$ precursors.[26] The as-prepared materials were finally calcined at 623 K for 1 h. All calcination treatments were performed under the flow of synthetic air.

Reaction setup

Photocatalytic activity measurements were performed at room temperature using a home-made continuous reaction system.[18] In brief, the setup consisted of a quartz reactor connected to a gas supply. The reaction products were monitored by an online MS (Pfeiffer Vacuum, Omnistar GSD 320) and the product quantification was verified by a GC (Agilent Technologies, micro-GC 490). Powder catalyst (20 mg, 0.6 g L^{-1}) was dispersed in ultrapure water (35 mL, Milli-Q). 0.01 M $AgNO_3$ aqueous solution was used for electron-trapped oxygen evolution studies. The suspension was kept under stirring and continuous N_2 gas flow (4.5 mL min^{-1}) during the reaction. The catalyst solution was purged with N_2 for 1 h prior to irradiation with a 400 W high-pressure Hg lamp (UV-Technik, without optical filter) at 8 cm distance from the reactor to avoid excessive heat-up and water evaporation. The Ga_2O_3-based materials are known to show photocatalytic activity with only UV light (<275 nm) and the test was performed without an optical filter.[18] The reactor temperature was monitored to be about 353 K during the reaction. Repeated light on/off cycles for 1.5 h of each on/off phase were studied for overall water splitting reaction. For the evaluation of O_2 evolution reaction in the presence of silver nitrate, the catalyst in solution was continuously irradiated for 4 h.

Materials characterization

Powder X-ray diffraction (PXRD) were performed on a Bruker D8 Advance power diffractometer with a vertical 2theta-theta goniometer in transmission configuration with Cu Kα radiation (λ=1.5406 Å). Maud software was used to perform phase quantification of the synthesised materials.[27] Instrumental broadening was firstly corrected to perform Rietveld refinement and phase quantification. XAS and valance-to-core (VtC)-XES measurements were performed at ID26 of the ESRF (Grenoble, France). The incoming energy was selected by the (111) reflection of a pair of cryogenically cooled Si crystals and the beam footprint on the sample was 1.0 x 0.2 mm^2. Higher harmonics were suppressed by three Si mirrors working at 2.5mrad. An emission spectrometer with four spherically bent (r=50mm, R=1000mm) analyser crystals in vertical Johann geometry was employed to select the Kβ fluorescence lines of Cr, Zn and Ga using the reflections Ge (333), Si (555) and Ge (555), respectively. HERFD-XANES were recorded on the maximum of the $Kβ_{1,3}$ line (9572.60 eV for Zn and 10265.37 eV for Ga; SI, Fig. S3. HERFD and total fluorescence detections are compared in Fig. S4) and by varying the incident energy from 10.36 to 10.46 keV (Ga), 9.65 to 9.75 keV (Zn) and 5.98 to 6.08 (Cr) in continuous scan mode. The spectra were not corrected for incident beam self-absorption (over-absorption) effects. Linear combination fitting was performed by using additional fitting parameters that account for the spectral distortion arising from self-absorption.

XES was measured for Ga and Zn K-edges at a fixed incident energy of 10.50 and 9.80 keV, respectively. VtC-XES were acquired from 10.28 to 10.40 keV (Ga) and 9.59 to 9.70 keV (Zn) with a step size of 0.30 eV. All samples and reference materials were measured *ex situ* in the form of pellet (13 mm diameter), containing 60 mg of material and 60 mg of cellulose. For *in situ* irradiation experiments, pellets (13 mm diameter) containing 200 mg of pure material were transiently irradiated with DH-2000 (Ocean Optics) UV-Vis-NIR deuterium-halogen light source while measuring 10 spectra under dark and then under light conditions. The light on-off cycles were repeated 11 times for the material without Rh-Cr (220 spectra in total; 120 s for each spectral acquisition) and 7 times for the samples containing Rh-Cr (140 spectra in total), and the subtle differences of the spectral features were studied by modulation excitation methodology explained in the following section. Athena was used to normalized the XANES spectra,[28] and for all the samples E_0 was set individually to the corresponding maximum position of the first derivative. Linear combination fitting (LCF) was performed on the normalized XANES spectra and two standards ZnO and $ZnGa_2O_4$ (Zn K-edge) and $ZnGa_2O_4$ and Ga_2O_3 (Ga K-edge) were used for the fitting in the range of 9.65-9.69 keV (Zn) and 10.36-10.40 keV (Ga).[29]

Modulation excitation spectroscopy (MES)

MES allows precise kinetic studies and sensitivity boosting of signals arising from transient processes.[25, 30, 31] In this study the latter advantage (typically 2-3 order of magnitude sensitivity boost) was exploited. The mathematical core of MES is phase sensitive detection (PSD, also called demodulation) as shown in Eq. (1), which converts time-domain response A(t) to a phase-domain response $A_k(φ_k^{PSD})$ with almost full reduction of

the static noise and signals unaffected by the external perturbation (here light on and off).[25, 30]

$$A_k(\phi_k{}^{PSD}) = \frac{2}{T}\int_0^T A(t)\ \sin(k\omega t + \phi_k{}^{PSD})dt \qquad (1)$$

The PSD analysis was performed at demodulation index k = 1.

Results and discussion

Photocatalytic activity of Zn-Ga$_2$O$_3$ and Rh-Cr/Zn-Ga$_2$O$_3$

First, effects of Zn-loading amount as well as addition of Rh-Cr promoters to Ga$_2$O$_3$ on photocatalytic water splitting activity were systematically studied. Fig. 1 compares the productivity of hydrogen and oxygen as a function of Zn-loading with/without addition of Rh-Cr co-catalyst. Bare Ga$_2$O$_3$, without Zn and Rh-Cr promoters, shows low H$_2$ productivity (0.16 mmol $g_{cat}{}^{-1}$ h^{-1}), although this productivity level is comparable to that of well-known Pt/TiO$_2$ photocatalyst (0.10 mmol $g_{cat}{}^{-1}$ h^{-1}).[32, 33] At 2-4 wt% Zn-loading, the H$_2$ productivity was enhanced reaching 1.1 mmol $g_{cat}{}^{-1}$ h^{-1}. However, the H$_2$ productivity drops at higher Zn-loadings (>20 wt%), as similarly reported by Wang *et al.* who observed the drop in the activity from 3 to 4 Zn-atom% (which would correspond to 1.1-1.4 wt% of Zn of this study).[34] Remarkably, the addition of Rh-Cr boosts the water splitting activity by almost one order of magnitude, while retaining the activity trends induced by the varying amount of Zn. The highest H$_2$ productivity of 9.0 mmol $g_{cat}{}^{-1}$ h^{-1} observed for Rh-Cr/4 wt% Zn-Ga$_2$O$_3$ was more than the sum of the Rh-Cr effect (3.3 mmol $g_{cat}{}^{-1}$ h^{-1}) and the Zn-effect (1.1 mmol $g_{cat}{}^{-1}$ h^{-1}), confirming the previously observed synergistic effects of the Zn and Rh-Cr promoters.[14, 18] Stoichiometric production of H$_2$ and O$_2$ was not achieved with higher H$_2$/O$_2$ ratio possibly due to the formation of peroxo-species,[33, 35] although we could not identify such species in the solution.
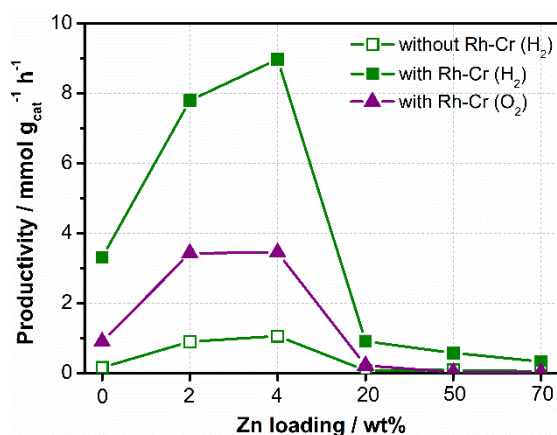
(below the detection limit of the GC) for confident quantification.

Geometrical and electronic structure changes by Zn-loading

The structures of the Zn-promoted Ga$_2$O$_3$ materials without Rh-Cr co-catalyst were studied by XRD, XAS, and XES to elucidate the changes induced by the Zn addition. The effects of Rh-Cr co-catalyst on the structure of the catalyst materials are considered to be solely electronic ones due to the low loading of Rh-Cr, as observed from the negligible influence on the characterization results by the presence of Rh-Cr (not shown here).

PXRD results (Fig. 2a) show that the Zn-Ga$_2$O$_3$ materials are composed of β-Ga$_2$O$_3$ and ZnGa$_2$O$_4$ phases at low Zn concentrations (2-4 wt%) in accordance with literature,[34] whereas in this work the presence of ZnO phase is also confirmed at high Zn-loading (≥20 wt%). The absence of the shifts of the β-Ga$_2$O$_3$ reflection peaks at all Zn-loadings indicates that Zn is not incorporated into the Ga$_2$O$_3$ lattice.[36] Electron microscopy and energy dispersive analysis indicate the presence of Zn elements near the material surface (Fig. S1). This suggests that ZnGa$_2$O$_4$ and ZnO are deposited on the surface of Ga$_2$O$_3$ as expected from the impregnation and subsequent calcination methods used to prepare the Zn-Ga$_2$O$_3$ materials. Quantitative phase analysis (Fig. S2) confirms that up to 4 wt% Zn-loading, Zn is present only as ZnGa$_2$O$_4$, while the amounts of both ZnGa$_2$O$_4$ and ZnO, particularly the latter, increase as the Zn-loading increases. Analysis of the HERFD-XANES spectra at Zn and Ga K-edge (Fig. 2b) by linear combination fitting, together with Zn K-edge VtC-XES (Fig. S5) and Zn K-edge EXAFS (Fig. S6) point to the identical conclusion, clearly showing how the Zn elements in the materials are present, either solely as ZnGa$_2$O$_4$ (2, 4 wt% Zn) in the vicinity of the Ga atoms with a creation of additional electronic states in the valance bands, or as a mixture of ZnGa$_2$O$_4$ and ZnO (≥20 wt% Zn).
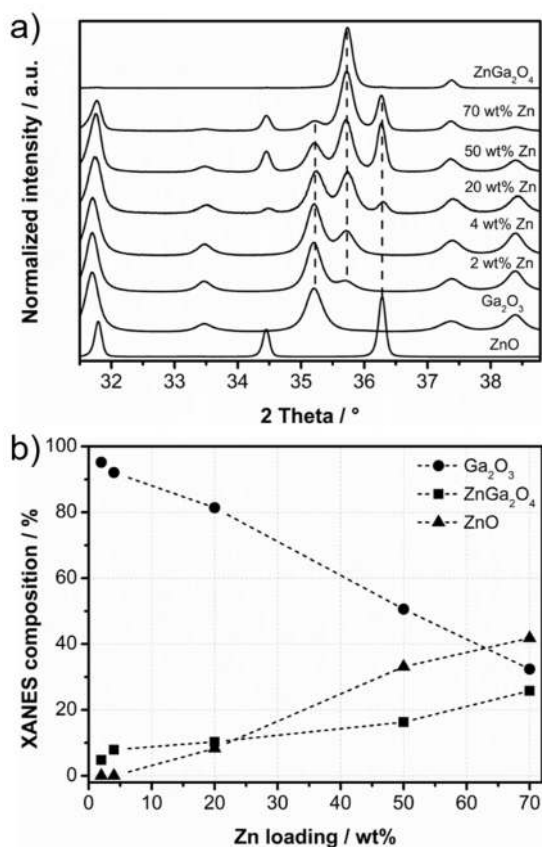

Fig. 1 H$_2$ (green) and O$_2$ (purple) productivity in the photocatalytic water splitting reaction using pure water for xZn-Ga$_2$O$_3$ and Rh-Cr/xZn-Ga$_2$O$_3$ (where x = 0, 2, 4, 20, 50, and 70 wt% of Zn). H$_2$/O$_2$ productivity was averaged from 4 runs by 1.5 h UV-Vis irradiation cycles. O$_2$ productivity for the materials without Rh-Cr is not shown because of the low amount of O$_2$

Fig. 2 a) PXRD patterns for Zn-modified Ga_2O_3 materials, including reference materials ZnO, $ZnGa_2O_4$, and Ga_2O_3. The dotted lines indicate Ga_2O_3 (35.2°), $ZnGa_2O_4$ (35.7°), and ZnO (36.3°) phases. b) Linear combination fitting analysis of Zn and Ga K-edge XANES spectra using $ZnGa_2O_4$ and ZnO, and $ZnGa_2O_4$ and Ga_2O_3 as standards to perform the fitting, respectively.

Furthermore, the integral electronic properties of Zn-modified Ga_2O_3 materials are studied by UV-Vis DRS through their optical properties (Fig. S7). The optical bandgap of Ga_2O_3 is barely modified by the Zn addition (from 4.58 to 4.55 eV). Therefore, the catalytic activity trends at different Zn-loading (Fig. 1) cannot be explained by the change in the bandgap. This is in accordance with the report by Wang *et al.* where Zn-Ga_2O_3 materials were studied for CO_2 reduction.[36] This also implies that the photon energy required to generate excitons (bound electron-hole pairs) is not strong enough to separate electrons and holes, which is required for photocatalytic reactions, and the functions and interface of different components of the photocatalyst facilitate the charge separation.

To gain precise insights into the electronic structures of the Zn-promoted materials, XAS and VtC-XES were employed to study unoccupied and occupied energy states, respectively, of Zn and Ga atoms within the materials (Fig. S8).[37] At both Zn K-edge (Fig. 3a) and Ga K-edge (Fig. 3b) the highest occupied energy level (VtC-XES results) are virtually unaltered among the reference materials. Nevertheless, it should be noted that electronic orbital mixing from *s* orbitals of O atom and *d* orbitals of Ga atom is observed at the VtC-XES Kβ" line of $ZnGa_2O_4$ (inset in Fig. 3a; the electronic structure assignments based on DFT calculations are shown in Fig. S5), affirming electronic

interaction and communication between Zn and Ga atoms in $ZnGa_2O_4$.

Clear differences are observed for the energy levels of unoccupied states at the Zn and Ga absorption edges. For the Zn K-edge, at small Zn concentrations (2 and 4 wt%) the lowest-unoccupied electronic states appear to be similar to those of $ZnGa_2O_4$ (Fig. S8a). At increasing Zn-loading where ZnO phase is more prominent, the absorption edges shift to lower energies, corresponding to smaller valance-conduction bandgaps (3.1 eV for ZnO, calculated from the difference between the maximum of the 1st derivative of the emission spectrum and the absorption edge as shown in Fig. S9). The bandgap of ZnO derived from the XAS-XES analysis that reflects the Zn p-projected density of states agrees with that of the optical bandgap (3.2 eV) determined by UV-Vis DRS. The small bandgap of ZnO (Fig. 3 and Fig. S9), its increasing light absorption at higher loading (Fig. S7) and the coexistence of $ZnGa_2O_4$ and Ga_2O_3 phases (Fig. 2a) suggest that ZnO covers $ZnGa_2O_4$-Ga_2O_3 at high Zn loading. This leads to inefficient use of photons for water splitting reactions (Fig. 1) because the ZnO conduction band energy is very close to the one required for H_2 evolution (-0.2 eV compared to 0 eV, respectively),[38] thus ZnO does not have the appropriate energy for water reduction upon light absorption.

On the other hand, the lowest-unoccupied energy states (XANES onset) of Ga are shifted toward higher energies with higher Zn content (Fig. S8b) as the amount of $ZnGa_2O_4$ increases (Fig. 2b), and pure $ZnGa_2O_4$ shows the highest K-edge energy (Fig. 3b, 4.42 eV as shown in Fig. S9). Thus, Ga in $ZnGa_2O_4$ has a considerably higher edge energy by ca. 1 eV compared to Ga_2O_3, implying a higher conduction band energy level of the former. These indications of higher conduction band energy level of $ZnGa_2O_4$, the slightly higher valance band energy by 0.05±0.01 eV (using the 1st moment of the Kβ$_{2,5}$ peak) determined for $ZnGa_2O_4$ with respect to that of β-Ga_2O_3 (smaller than 1.5 eV reported by valance band XPS),[34] and the Zn-loading-dependent coverage of $ZnGa_2O_4$ and ZnO over β-Ga_2O_3 surface point to the important roles of $ZnGa_2O_4$/Ga_2O_3 heterojunction as depicted in Fig. 4. Due to the similar optical bandgaps, excitons are generated in/on both materials and the electrons will migrate from $ZnGa_2O_4$ to Ga_2O_3 surface to catalyse reduction reactions and conversely the holes migrate from Ga_2O_3 to $ZnGa_2O_4$ to catalyse oxidation reactions. The creation of the heterojunction explains the reported longer life-time of photogenerated electrons and holes by transient spectroscopic methods.[18, 34] Adequate amount of $ZnGa_2O_4$ should be present on Ga_2O_3 to efficiently create the heterojunction, while sufficiently large area of Ga_2O_3 should also be exposed to catalyse hydrogen evolution reactions. On the other hand, upon ZnO formation on the catalyst surface due to excessive Zn-loading, light is merely absorbed by the material without energy harvesting for water splitting (Fig. 4).
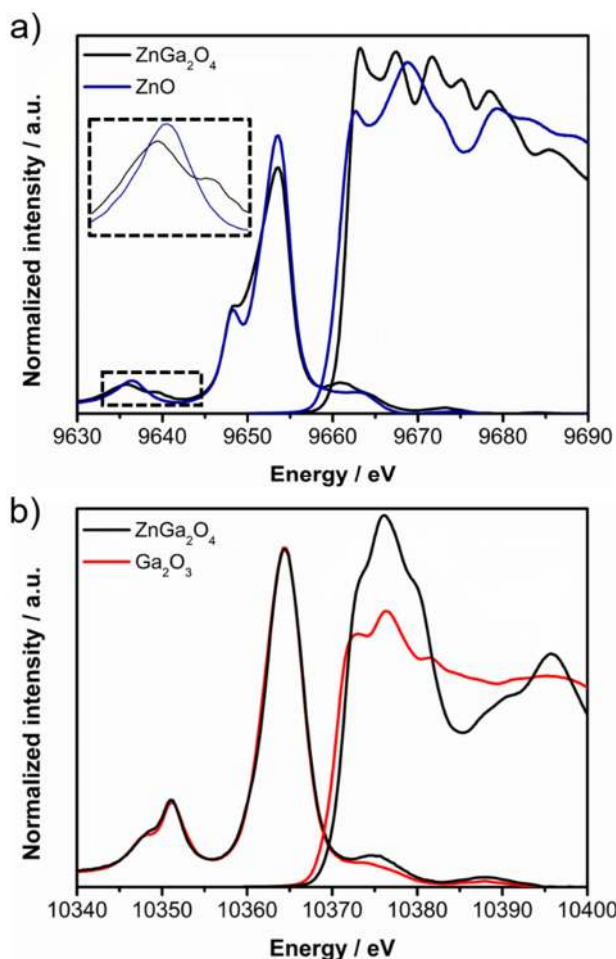
Fig. 3 XAS and VtC-XES spectra for a) Zn K-edge and b) Ga K-edge. Pure $ZnGa_2O_4$ (black), ZnO (blue), and Ga_2O_3 (red). Spectral intensity was normalized to the spectral area.
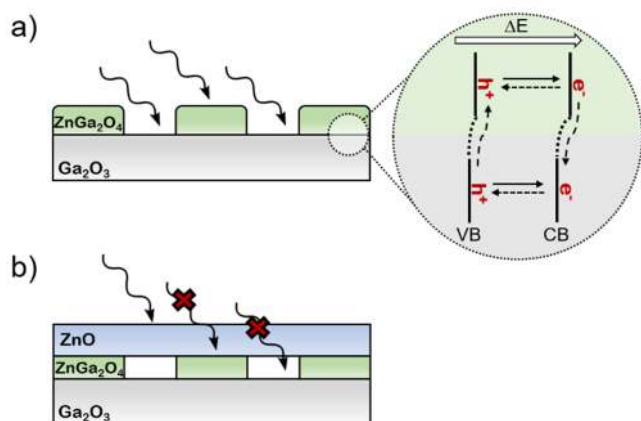

Fig. 4 Schematic of light absorption for Zn-Ga_2O_3 materials with a) low Zn loadings (2-4 wt%) showing the electron and hole migrations between the $ZnGa_2O_4$/Ga_2O_3 heterojunction, and b) high Zn loadings (≥20 wt%).

Role of Rh-Cr co-catalyst

As presented in Fig. 1, a small amount of Rh-Cr drastically boosts the catalytic activity of Ga_2O_3 and Zn-Ga_2O_3 materials. Promoting effects of metal co-catalysts in photocatalytic reactions are generally attributed to their function as electron trap and sink.[9, 16, 39] To firmly understand and attribute the function of Rh-Cr co-catalyst, water splitting activity and structural changes of 4 wt% Zn-Ga_2O_3 with/without Rh-Cr were studied using silver nitrate as electron scavenger.

Photocatalytic experiments in the presence of silver nitrate (Fig. 5b) show fully suppressed H_2 production as anticipated by the efficient electron intercept by Ag^+ at the location where free electrons are concentrated and released. To our surprise, only a small amount of O_2 was detected for both materials despite the well-documented function of Ag^+ to enhance water oxidation activity of photocatalysts.[40, 41] Also, the O_2 productivity with and without Rh-Cr co-catalyst was similar, indicating disabled function of Rh-Cr in the presence of Ag^+. STEM (Fig. S10) and Cr K-edge XANES (Fig. S11) of the Rh-Cr/Zn-Ga_2O_3 material after the reaction in the presence of $AgNO_3$ clearly show that Ag deposition occurs around the Cr_xO_y particles, and also the oxidation of Cr takes place (in comparison to reference spectra the initial +3 oxidation number of Cr increases, although it is not exactly +6, Fig. S11).[26] Similarly to Cr, small changes in the electronic state of Rh were indicated after Ag deposition from the Rh K-edge XANES (Rh oxidation number is slightly oxidized, although initially is not exactly 3+, Fig. S12),[26] although Rh and its spatial distribution could not be studied by TEM due to the low Rh loading (0.5 wt%). Thus Rh-Cr, particularly Cr, is the site where electrons are released for reduction reactions and hence Ag is selectively deposited on Cr oxide particles. The reduction reaction proceeds in a sacrificial manner for Cr (i.e. Cr is self-oxidized) and thus Ag reduction is efficient through the reducing power of Cr_xO_y sites. This explains the lowered ability of the catalyst for charge separation and thus leading to less efficient electron trap after Ag deposition at Rh-Cr sites. Furthermore, the lowered efficiency for charge separation by ineffective function of Rh-Cr by Ag deposition explains the suppressed oxygen formation in the presence of Ag^+ (Fig 5a vs. 5b).

Ag deposition under illumination (i.e. photodeposition) is shown to be site selective and it is expected to uniquely influence the water splitting activity. This was verified by performing the photocatalytic water splitting tests in pure water using the material after Ag photodeposition for 30 min (20 wt% Ag determined by EDX) and using a comparable material prepared by the impregnation method at the same Ag loading (Fig. 5c and 5d). In all cases, lower activity is found in comparison to the materials without Ag deposition (Fig. 5a). The most important difference is observed for the Rh-Cr promoted catalyst where Ag-impregnated catalyst showed relatively high H_2 productivity (4.9 mmol g_{cat}^{-1} h^{-1}) in contrast to the minor activity of the Ag-photodeposited one (0.8 mmol g_{cat}^{-1} h^{-1}). Microscopic study shows that the Ag deposition by the impregnation method leads more homogenous distribution of Ag and not site-selective (Fig. S13). Thus, the poisoning of the

active sites is not prominent. On the other hand, the catalytic activity is largely suppressed when Ag selectively covers Rh-Cr co-catalyst (speculated for Rh).
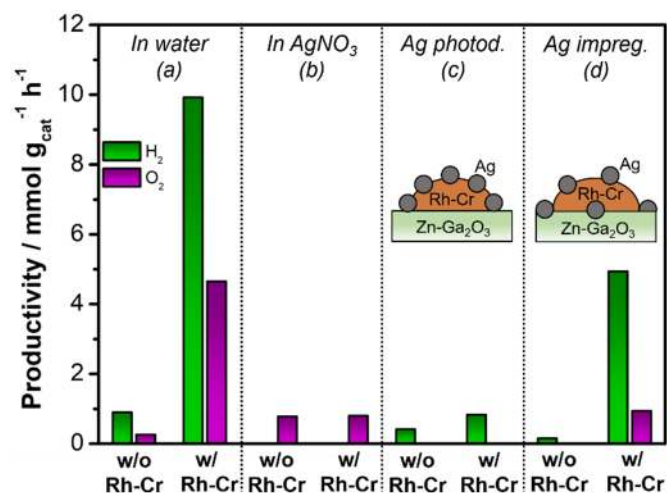

Fig. 5 H_2 (green) and O_2 (purple) productivity of 4 wt% Zn-Ga$_2$O$_3$ with and without Rh-Cr in the photocatalytic water splitting reaction; (a) in pure water, (b) in the presence of 0.01 M AgNO$_3$, (c) in pure water after 20 wt% Ag-photodeposition and (d) in pure water after 20 wt% Ag-impregnation. The duration of photocatalytic test was 1.5 h (averaged from 4 runs) except for the case in the presence of AgNO$_3$ (b) for which the test was performed only for 30 min due to fast deactivation induced by Ag deposition on the catalysts. The small difference in the catalytic activity (a) and those shown in Fig. 1 is due to the different batch of catalysts synthesized and possibly to the experimental error of different photocatalytic tests. Nevertheless, the difference is within the levels of common tolerance (about 10%).

Synergistic effects of Rh-Cr and Zn

Fig. 5 also shows that O_2 productivity is fully suppressed when the function of Rh-Cr is disabled by the Ag deposition, affirming that the charge separation facilitated by the role of Rh-Cr as electron sink (reduction site) and the function of Zn through the formation of ZnGa$_2$O$_4$/Ga$_2$O$_3$ heterojunction (Fig. 4) are interlinked, as also evidenced by the synergistic effects of Zn and Rh-Cr in the photocatalytic activity (Fig. 1). With the aim to directly sense the influence of Rh-Cr co-catalyst on the electronic structure of Zn atoms as a proof of the synergistic interactions, here the unoccupied state electronic structures of Zn are studied by XANES with *in situ* illumination.

As expected, the XANES difference spectra of Zn-Ga$_2$O$_3$ and Rh-Cr/Zn-Ga$_2$O$_3$ between the dark and illuminated conditions are very small, close to the level of noise even after signal to noise (S/N) improvement by averaging the respective spectra before subtraction (Fig. 6a). To drastically boost the sensitivity, the experiments are performed periodically in light-on/off cycles and the resulting spectra were averaged into one light-on/off cycle. Then the averaged spectra were treated by the mathematical engine of modulation excitation spectroscopy, phase sensitive detection (PSD) (Fig. 6b and Fig. S14).[25] PSD

highlights only the intensity which varies at the same frequency as the light on/off stimulus, thus effectively eliminates uncorrelated noise and time-independent static signals. Only the phase-domain spectra at ϕ_{PSD} = 0 are presented since this would be equivalent to the difference spectra of the catalyst under-light minus under-dark. The improvement in S/N is evident, although the spectral features are very small. The physical nature of the small spectral characteristics is verified by the so-called in-phase angle analysis (Fig. S14-iii), clearly showing distinct phase angles for each peak (continuously shifting phase angles are due to peak overlaps as expected in XANES, also serving as the proof of the physical nature of the low intensity signals and not of noise).

Two important observations can be made from this light-on/off XANES study. First, the electronic structure of Zn atom, which is present as ZnGa$_2$O$_4$ (*vide supra*), is perturbated by the illumination. This is an indirect evidence of the charge separation at ZnGa$_2$O$_4$ by which the electronic structure of Zn is also influenced to vary. Another very striking observation is the effect of Rh-Cr on the degree of the change. The degree of change in the Zn electronic structure is about double by the presence of Rh-Cr co-catalyst. Detailed spectral analysis (i.e. how the Zn orbitals are altered) is beyond the scope of this work; nevertheless, the clearly different spectral features (e.g. where the maxima appear for the two materials) indicate the electronic structure of Zn atom under illumination is different with/without Rh-Cr, possibly due to the different degree of charge separation. This is the first and a clear proof that the charge separation facilitated by Rh-Cr communicates with the electronic structure of Zn. Also, the results imply that the physical vicinity of Rh-Cr is important and how and where Rh-Cr are deposited (e.g. on Ga$_2$O$_3$, ZnGa$_2$O$_4$ or at their interface) matter for the photocatalytic activity.

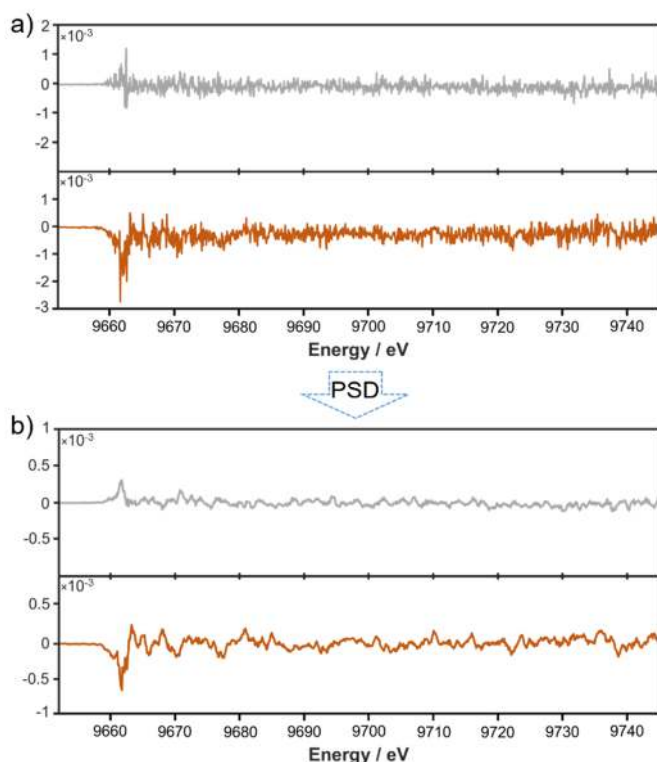Fig. 6 a) Averaged Zn K-edge HERDF-XANES spectra, light off subtracted from light on cycle, and b) phase-domain response with k = 1 of 4 wt% Zn-modified Ga_2O_3 (grey), and Rh-Cr/4 wt% Zn-Ga_2O_3 (brown).

Conclusions

Zn and Rh-Cr co-catalysts greatly influence the photocatalytic water splitting activity of Ga_2O_3 and their synergistic function is confirmed. At the optimum Zn-loading (2-4 wt%) the formation of the $ZnGa_2O_4$/Ga_2O_3 heterojunction, with an appropriate exposure of both materials for the redox reactions, is favoured facilitating the charge transfer and separation between the two semiconductor materials and thus enhancing the photocatalytic activity. At higher Zn-loading (≥20 wt%) ZnO is formed covering the $ZnGa_2O_4$ and Ga_2O_3 surface and negatively influences the photocatalytic activity due to the light absorption properties and water splitting activity of ZnO. The role of Rh-Cr as electron trapping sites is evidenced by the studies in the presence of Ag^+, clearly showing the poisoning of the Rh-Cr active sites after Ag deposition. By depositing Ag in a selective (photodeposition) and non-selective (impregnation) fashions and detailing the electronic structure change of Cr, the function of Rh-Cr co-catalyst in water splitting reaction was affirmed. Finally, the concerted actions between the electron sink (Rh-Cr) and the $ZnGa_2O_4$/Ga_2O_3 heterojunction are proven by *in situ* illumination modulation excitation XAS spectroscopy. The subtle electronic structure change of Zn atoms in $ZnGa_2O_4$ under illumination is uncovered. The degree of the change is boosted by the presence of Rh-Cr, serving as a direct proof of communication and synergy of Zn and Rh-Cr co-catalysts on the electronic structure level under photocatalytic conditions.

Conflicts of interest

There are no conflicts to declare.

References

1. M. D. Hernandez-Alonso, F. Fresno, S. Suarez and J. M. Coronado, *Energ. Environ. Sci.*, 2009, **2**, 1231-1257.
2. A. Kudo and Y. Miseki, *Chem. Soc. Rev.*, 2009, **38**, 253-278.
3. K. Maeda and K. Domen, *J. Phys. Chem. Lett.*, 2010, **1**, 2655-2661.
4. A. Fujishima and K. Honda, *Nature.*, 1972, **238**, 37-38.
5. A. J. Bard and M. A. Fox, *Accounts. Chem. Res.*, 1995, **28**, 141-145.
6. A. L. Linsebigler, G. Lu and J. T. Yates, *Chem. Rev.*, 1995, **95**, 735-758.
7. K. Maeda and K. Domen, *J. Phys. Chem. C.*, 2007, **111**, 7851-7861.
8. F. E. Osterloh, *Chem. Mater.*, 2008, **20**, 35-54.
9. G. Liu, L. Wang, H. G. Yang, H.-M. Cheng and G. Q. Lu, *J. Mater. Chem.*, 2010, **20**, 831-843.
10. T. Yanagida, Y. Sakata and H. Imamura, *Photocatalytic Decomposition of H2O into H2 and O2 over Ga2O3 Loaded with NiO*, 2004.
11. K. Maeda, K. Teramura, H. Masuda, T. Takata, N. Saito, Y. Inoue and K. Domen, *J. Phys. Chem. B.*, 2006, **110**, 13107-13112.
12. K. Maeda, K. Teramura, D. Lu, T. Takata, N. Saito, Y. Inoue and K. Domen, *Nature.*, 2006, **440**, 295.
13. K. Maeda, K. Teramura, D. Lu, N. Saito, Y. Inoue and K. Domen, *Angew. Chem. Int. Edit.*, 2006, **45**, 7806-7809.
14. Y. Sakata, Y. Matsuda, T. Nakagawa, R. Yasunaga, H. Imamura and K. Teramura, *ChemSusChem.*, 2011, **4**, 181-184.
15. Y. Sakata, T. Nakagawa, Y. Nagamatsu, Y. Matsuda, R. Yasunaga, E. Nakao and H. Imamura, *J. Catal.*, 2014, **310**, 45-50.
16. K. Shimura, T. Yoshida and H. Yoshida, *J. Phys. Chem. C.*, 2010, **114**, 11466-11474.
17. Y. Sakata, Y. Matsuda, T. Yanagida, K. Hirata, H. Imamura and K. Teramura, *Catal. Lett.*, 2008, **125**, 22-26.
18. A. Bazzo and A. Urakawa, *Catal. Sci. Technol.*, 2016, **6**, 4243-4253.
19. P. Glatzel and U. Bergmann, *Coordin. Chem. Rev.*, 2005, **249**, 65-95.

20. J. Szlachetko and J. Sá, *CrystEngComm.*, 2013, **15**, 2583-2587. 21. E. Gallo and P. Glatzel, *Adv. Mater.*, 2014, **26**, 7730-7746.

22. R. López and R. Gómez, *J. Sol-Gel. Sci. Techn.*, 2012, **61**, 1-7.

23. A. B. Murphy, *Sol. Energ. Mat. Sol. C.*, 2007, **91**, 1326-1337.

24. K. Wojtaszek, K. Tyrala, J. Czapla-Masztafiak, J. Sa and J. Szlachetko, *Chem. Phys. Lett.*, 2016, **664**, 73-76.

25. A. Urakawa, T. Bürgi and A. Baiker, *Chem. Ehg. Sci.*, 2008, **63**, 4902-4909.

26. K. Maeda, K. Teramura, D. Lu, T. Takata, N. Saito, Y. Inoue and K. Domen, *J. Phys. Chem. B.*, 2006, **110**, 13753-13758.

27. L. Lutterotti, R. Ceccato, R. Dal Maschio and E. Pagani, *Mater. Sci. Forum.*, 1998, **278-281**, 87-92.

28. B. Ravel and M. Newville, *J. Synchrotron. Radiat.*, 2005, **12**, 537-541.

29. T. Ressler, J. Wong, J. Roos and I. L. Smith, *Environ. Sci. Technol.*, 2000, **34**, 950-958.

30. D. Baurecht and U. P. Fringeli, *Rev. Sci. Instrum.*, 2001, **72**, 3782-3792.

31. A. Urakawa, T. Bürgi and A. Baiker, *Chem. Phys.*, 2006, **324**, 653-658.

32. X. Chen, S. Shen, L. Guo and S. S. Mao, *Chem. Rev.*, 2010, **110**, 6503-6570.

33. S. Tabata, H. Nishida, Y. Masaki and K. Tabata, *Catal. Lett.*, 1995, **34**, 245-249.

34. X. Wang, S. Shen, S. Jin, J. Yang, M. Li, X. Wang, H. Han and C. Li, *Phys. Chem. Chem. Phys.*, 2013, **15**, 19380-19386.

35. J. C. Hill and K.-S. Choi, *J. Phys. Chem. C.*, 2012, **116**, 7612-7620.

36. Z. Wang, K. Teramura, Z. Huang, S. Hosokawa, Y. Sakata and T. Tanaka, *Catal. Sci. Technol.*, 2016, **6**, 1025-1032.

37. P. Glatzel, T. C. Weng, K. Kvashnina, J. Swarbrick, M. Sikora, E. Gallo, N. Smolentsev and R. A. Mori, *J. Electron. Spectrosc.*, 2013, **188**, 17-25.

38. T. Inoue, A. Fujishima, S. Konishi and K. Honda, *Nature.*, 1979, **277**, 637.

39. J. Disdier, J.-M. Herrmann and P. Pichat, *J. Chem. Soc. Farad. T. 1.*, 1983, **79**, 651-660.

40. K. Maeda, H. Hashiguchi, H. Masuda, R. Abe and K. Domen, *J. Phys. Chem. C.*, 2008, **112**, 3447-3452.

41. B. Ohtani, S. Zhang, J. Handa, H. Kajiwara, S. Nishimoto and T. Kagiya, *J. Photoch. Photobio. A.*, 1992, **64**, 223-230.

Supporting Information

Synergistic interplay of Zn and Rh-Cr promoters on

Ga₂O₃ based photocatalyst for water splitting

Marta Borges Ordoño[a], Shunsaku Yasumura[a], Pieter Glatzel[b],

and Atsushi Urakawa*[a]

[a]Institute of Chemical Research of Catalonia (ICIQ), The Barcelona Institute of Science and Technology,

Tarragona, 43007, Spain

*[b]ESRF - The European Synchrotron, Grenoble, 38043, France*

E-mail: aurakawa@iciq.es

MATERIALS CHARACTERIZATION

UV-Vis DRS measurements were performed on a Shimadzu UV-2401PC spectrophotometer with D_2 and W lamps as light sources, and a photomultiplier detector. Solid samples were introduced in a round holder with a fused silica window on an integrating sphere attachment ISR-240A from Shimadzu. $BaSO_4$ was used as internal standard and spectra were collected between 240 and 800 nm. Band gap (E_g) was calculated from the slope intersection of the normalized Kubelka-Munk absorption spectrum.

Scanning transmission electron microscopy (STEM) was measured in annular dark-filed imaging mode (HAADF) in a high-resolution FEI Tecnai F20 STEM microscope at ICN2 (Barcelona). Chemical analysis and chemical mapping were performed by energy dispersive X-ray spectroscopy (EDX) and electron energy loss spectroscopy (EELS), respectively. 4 wt% $Zn-Ga_2O_3$ and $Rh-Cr/4wt\%$ $Zn-Ga_2O_3$ materials prepared in ethanol solution and were deposited on the a TEM support grid.

Cr and Rh elements were studied at their corresponding K-edge energies 5.99 and 23.22 keV, respectively. HERFD-XANES were measured from 5.98 to 6.08 keV (Cr) and 23.18 to 23.40 keV (Rh); with a step size for Cr of 0.1 eV and 0.05 eV for Rh. The spectrometer was equipped with four spherical Ge (333) crystal for Cr, and a diode IF3 with Cu+Ni filter was used for Rh detection. All the samples and reference materials were measured ex situ in the form of pellet (13 mm diameter), containing 60 mg of material and 60 mg of cellulose.
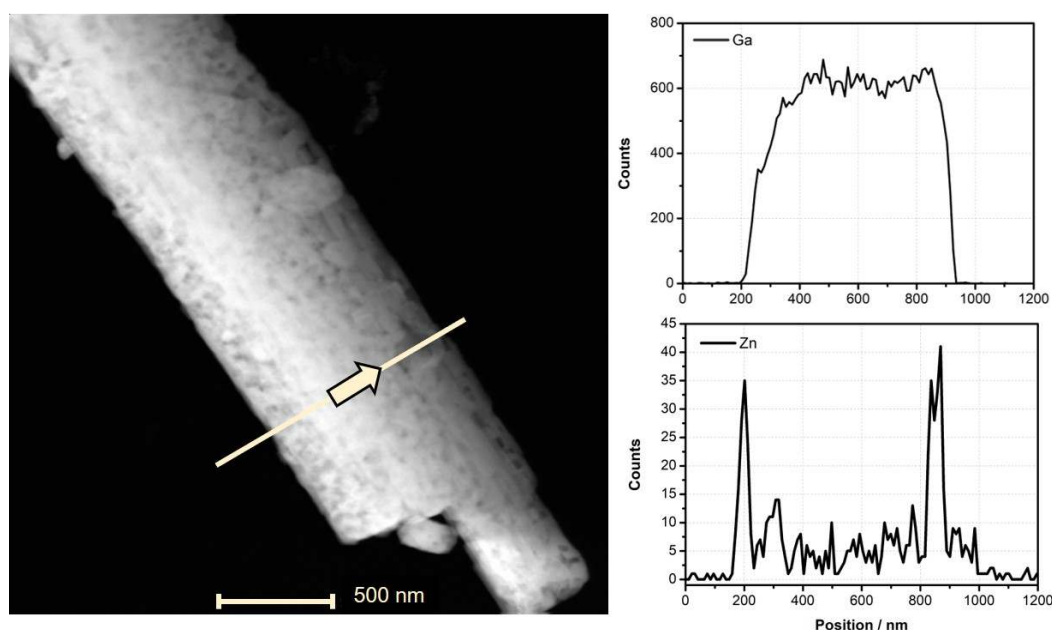
Fig. S1 (left) STEM-HAADF image of 4 wt% $Zn-Ga_2O_3$ material, with the transversal line indicating where EDX was measured. (right) Elemental profiles of Ga (top) and Zn (bottom) along the transversal line.
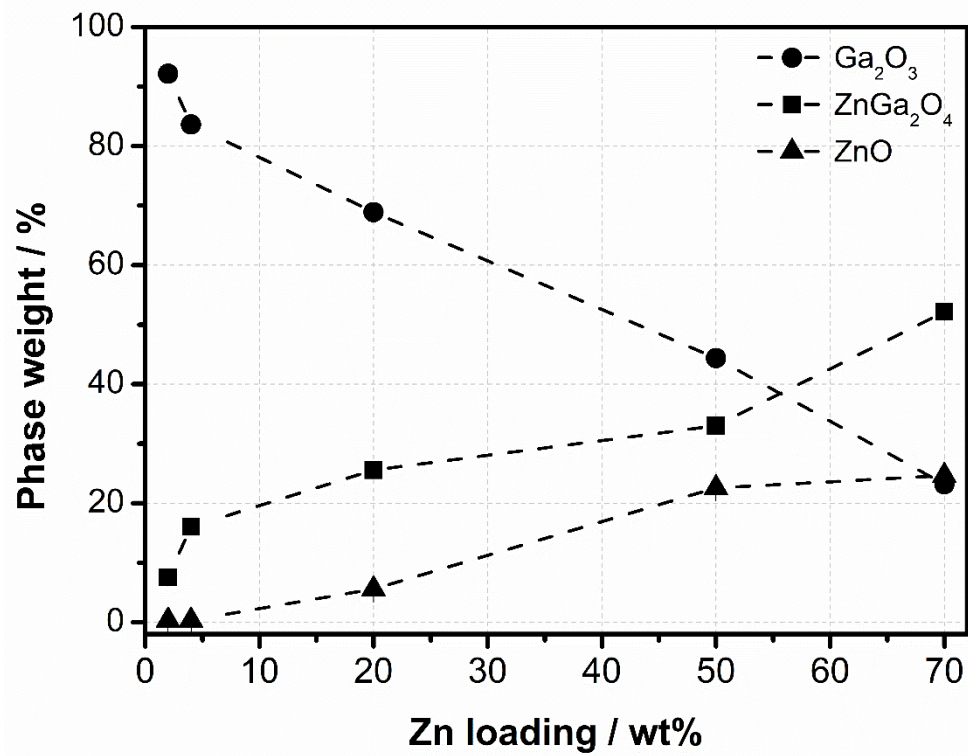
Fig. S2 Quantitative phase analysis of the XRD data for xZn-modified Ga_2O_3 photocatalysts where x= 2, 4, 20, 50, and 70 wt% of Zn.

Table. S1 Relative shift calculated from Kβ lines using the center of mass for Zn-Kedge (top) and Ga-Kedge (bottom).

Sample	Kβ	Center of mass (eV)	Relative shift (eV)
ZnO	1 2	9571.863 9571.863	0
ZnGa$_2$O$_4$	1 2	9571.832 9571.832	0
2 wt% Zn-Ga$_2$O$_3$	1 2	9571.842 9571.844	0.002
4 wt% Zn-Ga$_2$O$_3$	1 2	9571.842 9571.842	0
20 wt% Zn-Ga$_2$O$_3$	1 2	9571.855 9571.852	0.003
50 wt% Zn-Ga$_2$O$_3$	1 2	9571.854 9571.859	0.005
70 wt% Zn-Ga$_2$O$_3$	1 2	9571.853 9571.854	0.001

Sample	Kβ	Center of mass (eV)	Relative shift (eV)
Ga$_2$O$_3$	1	10264.09	0
	2	10264.09	
ZnGa$_2$O$_4$	1	10264.07	0
	2	10264.07	
2 wt% Zn-Ga$_2$O$_3$	1	10264.11	0.01
	2	10264.12	
4 wt% Zn-Ga$_2$O$_3$	1	10264.11	0
	2	10264.11	
20 wt% Zn-Ga$_2$O$_3$	1	10264.13	0
	2	10264.13	
50 wt% Zn-Ga$_2$O$_3$	1	10264.12	0.01
	2	10264.13	
70 wt% Zn-Ga$_2$O$_3$	1	10264.06	0

	2	10264.06	
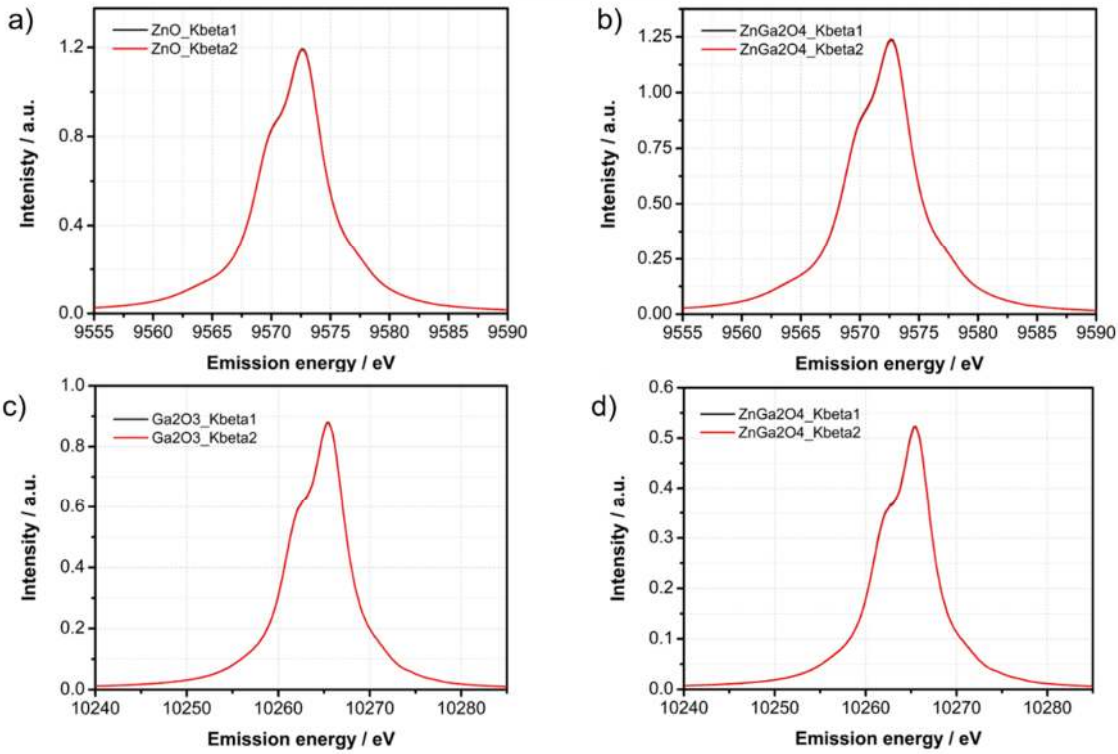
Fig. S3 Comparison of successive scans of Kβ main line for Zn K-edge a) ZnO and b) ZnGa$_2$O$_4$ and Ga K-edge c) Ga$_2$O$_3$ and d) ZnGa$_2$O$_4$.
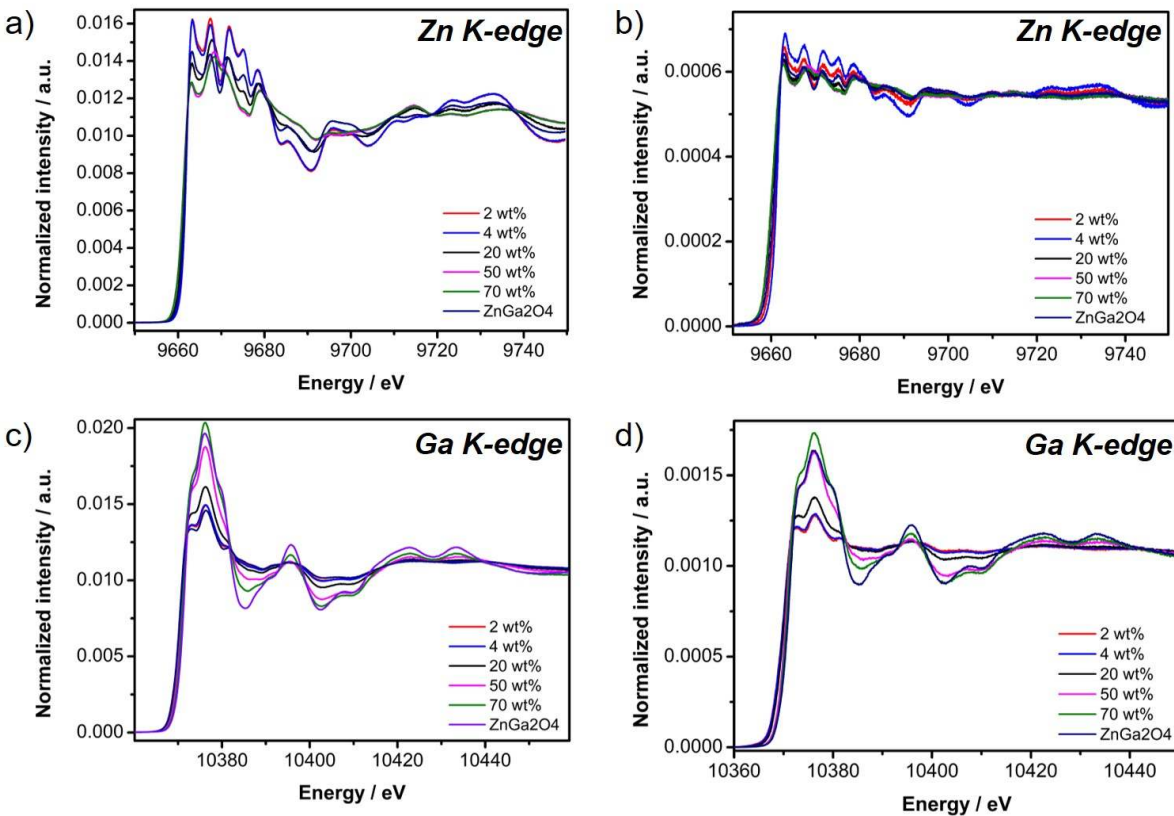
Fig. S4 XANES for Zn K-edge and Ga K-edge comparing HERFD scans (a and c) with total fluorescence scans (b and d).

The performance of density functionals PBE and PBE0 was compared, but due to the high computational cost of PBE0, PBE was applied to perform the cell optimization of the ZnO, Ga_2O_3, and $ZnGa_2O_4$ structures. First, the atomic positions in the corresponding cells and lattice parameters were optimized using PBE. After this, the energy calculations were performed by PBE0 to obtain more accurate DOS with the atomic positions and lattice parameters calculated above.

Table S2. DOS calculations details

| Package			
	CASTEP		
Conditions of Cell optimization			
	ZnO	Ga_2O_3	$ZnGa_2O_4$
Functional	PBE	PBE	PBE
Energy tolerance (eV/atom)	1.00E-05	1.00E-05	1.00E-05
Max. force(eV/Å)	0.03	0.03	0.03
Max. stress (Gpa)	0.05	0.05	0.05
Max. displacement (Å)	0.001	0.001	0.001
Energy cutoff (eV)	750	800	800
K-mesh	5x5x4	5x5x2	3x3x3
SCF tolerance (eV/atom)	1.00E-06	1.00E-06	1.00E-06
Conditions of SCF by PBE0			
	ZnO	Ga_2O_3	$ZnGa_2O_4$
Functional	PBE0	PBE0	PBE0
Energy cutoff (eV)	600	600	600
K-mesh	4x4x2	4x4x2	3x3x3
SCF tolerance (eV/atom)	2.00E-06	2.00E-06	2.00E-06

The coverage or phase transformation of $ZnGa_2O_4$ into ZnO could be further determined by looking deeper into the Zn K-edge VtC-XES region. Typically, VtC spectra has two lines corresponding to $K\beta_{2,5}$ (located below the Fermi level) and $K\beta''$ (cross over) at lower fluorescence energy.[1] At low Zn concentrations (2 and 4 wt%) the $K\beta''$ line was split because of the interaction from the metal (Zn) with s orbitals of O and d orbitals of Ga (**Fig. S5**), this result was supported by the density of states calculations on the reference materials (details of calculation shown in **Table S2**). On the contrary, at high Zn loadings where ZnO phase was detected the $K\beta''$ line only contains the contribution of s orbitals from O, indicating that first coordination shell of Zn atoms does not contain Ga atoms which might be attributed to the reduced accessibility of Zn atoms to the Ga_2O_3 surface, in agreement with the EXAFS analysis (**Fig. S6**). In addition, the third emission line due to multielectron transitions (ME) from the emitted and absorbed photoelectrons is observed in the Zn K-edge VtC spectra (**Fig. S5**). The intensity of this ME region is located above the Zn absorption edge energy and decreases with ZnO formation following the same trend that the photocatalytic activity results. However, correlation with the catalytic results are not discussed here because of the self-absorption effects that could also contribute to the ME intensity.[2, 3]
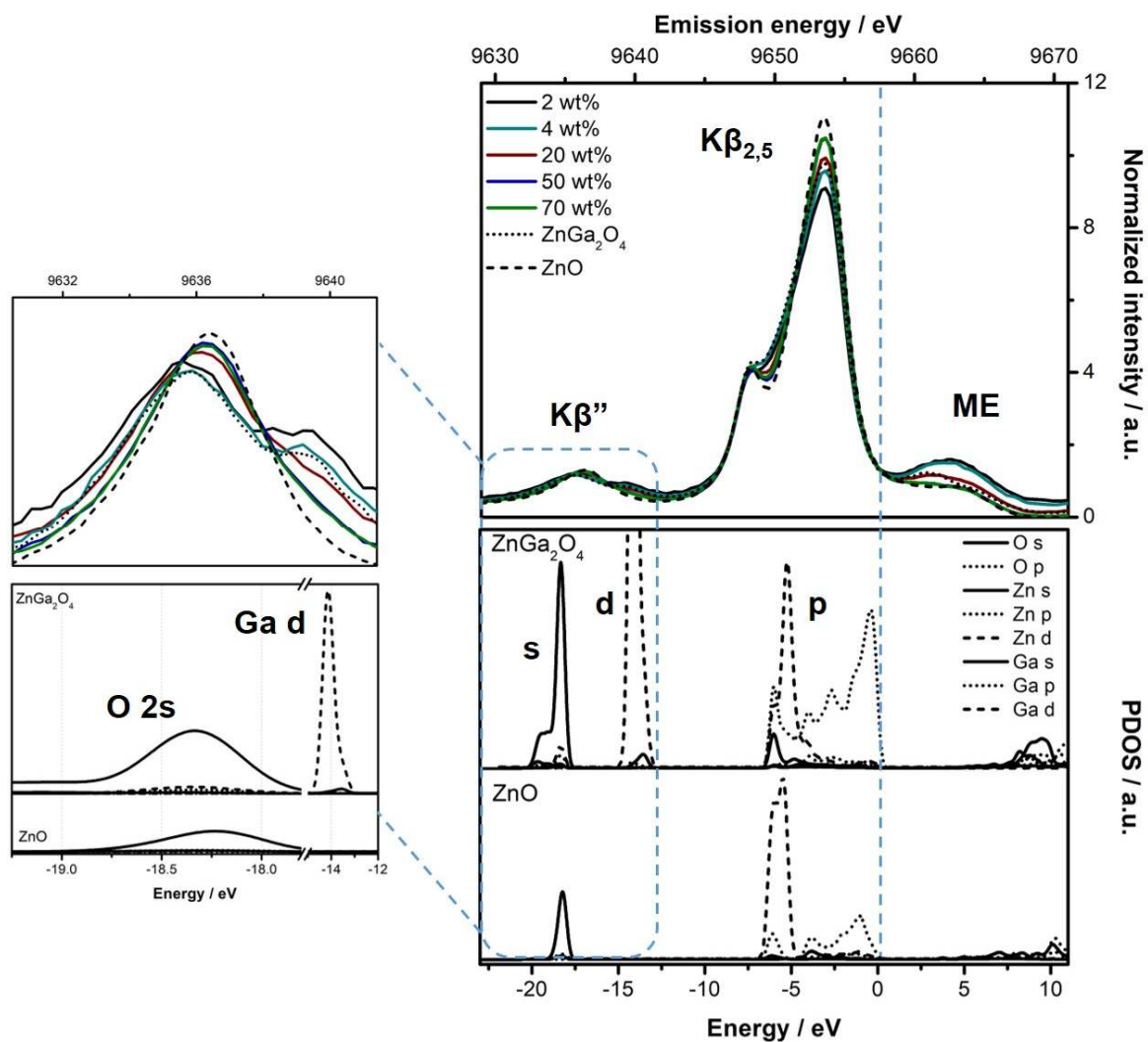
Fig. S5 Zn K-edge VtC-XES with normalized intensity to the spectral area (top). PDOS calculations for O, Ga, and Zn where mainly s and p regions correspond to the Kβ" and Kβ$_{2,5}$ lines, respectively. The dashed blue line indicates the Fermi level, and the zoomed region corresponds to Kβ".
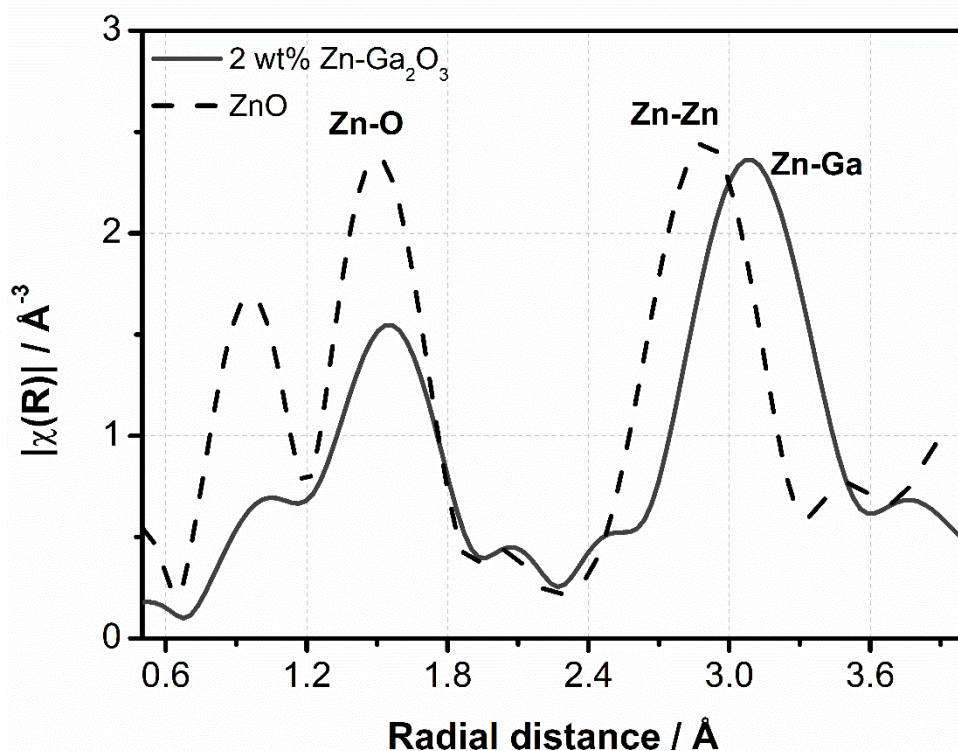
Fig. S6 EXAFS analysis of low Zn content Ga_2O_3 (2 wt%) compared to ZnO (dotted line) reference material. Self-absorption correction was performed on the ZnO EXAFS data by using the Fluo algorithm (Haskel, 1999).
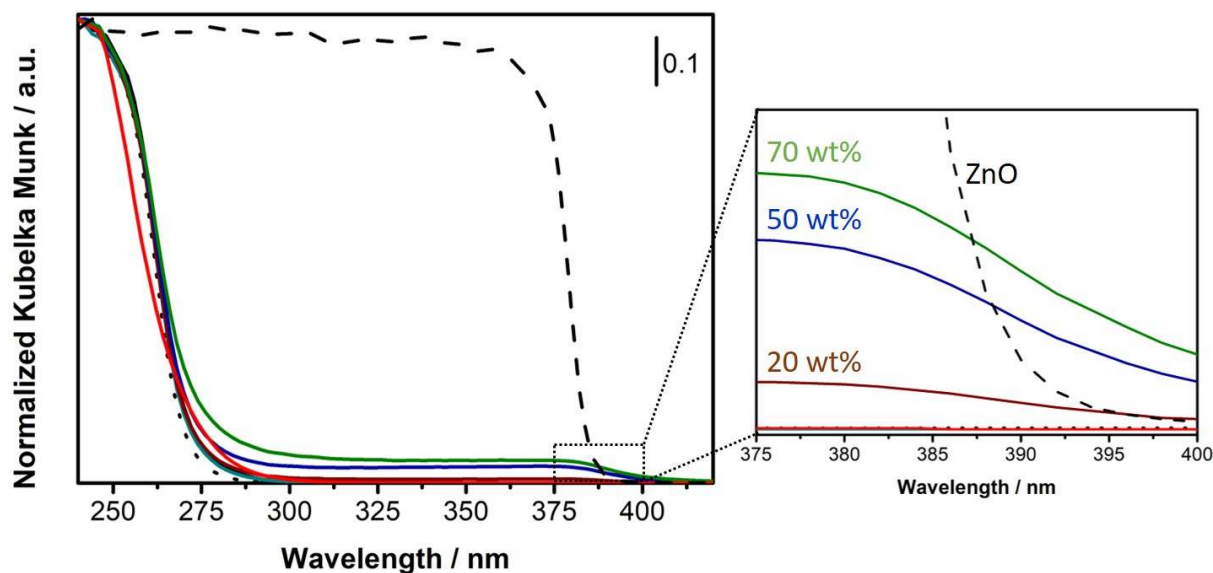
Fig. S7 UV-Vis DR spectra of xZn-Ga_2O_3 materials with x = 2 (black), 4 (cyan), 20 (maroon), 50 (blue) and 70 (green) and of reference materials, $ZnGa_2O_4$ (red), Ga_2O_3 (dotted line) and ZnO (dashed line). Spectra are shown in normalized Kubelka-Munk absorbance unit and the bandgaps were calculated from the slope of the adsorption spectra. Zoomed plot shows the region highlighting light absorption by ZnO.

For both Zn K-edge (**Fig. S8a**) and at Ga K-edge (**Fig. S8b**), opposite trends are observed for the unoccupied energy levels at the Zn and Ga absorption edges (inset plots, **Fig. S8)**. For the Zn K-edge, at small Zn concentrations (2 and 4 wt%) the lowest-unoccupied electronic sates appear to be comparable to those of $ZnGa_2O_4$ (**Fig. S8a**), while at increasing Zn-loading where ZnO phase is more prominent, the absorption edges shift to lower energies, corresponding to smaller valance-conduction band gaps. This agrees with the UV-Vis DRS study (**Fig. S7**), at high Zn loading (≥20 wt%) a weak absorption extending in the visible region appears clearly due to the presence of ZnO, with the optical bandgap of 3.0-3.1 eV.

In contrast, the lowest-unoccupied energy states of Ga are shifted toward higher energies at higher Zn content, pure $ZnGa_2O_4$ shows the highest lowest-unoccupied energy state (**Fig. S8b**). The small shift of the unoccupied energy states of Ga at low Zn concentrations (e.g. energy difference between Ga_2O_3 and 4 wt% $Zn-Ga_2O_3$ is 0.06 eV) is likely attributed to the minor contribution of $ZnGa_2O_4$ phase for such Zn loadings.
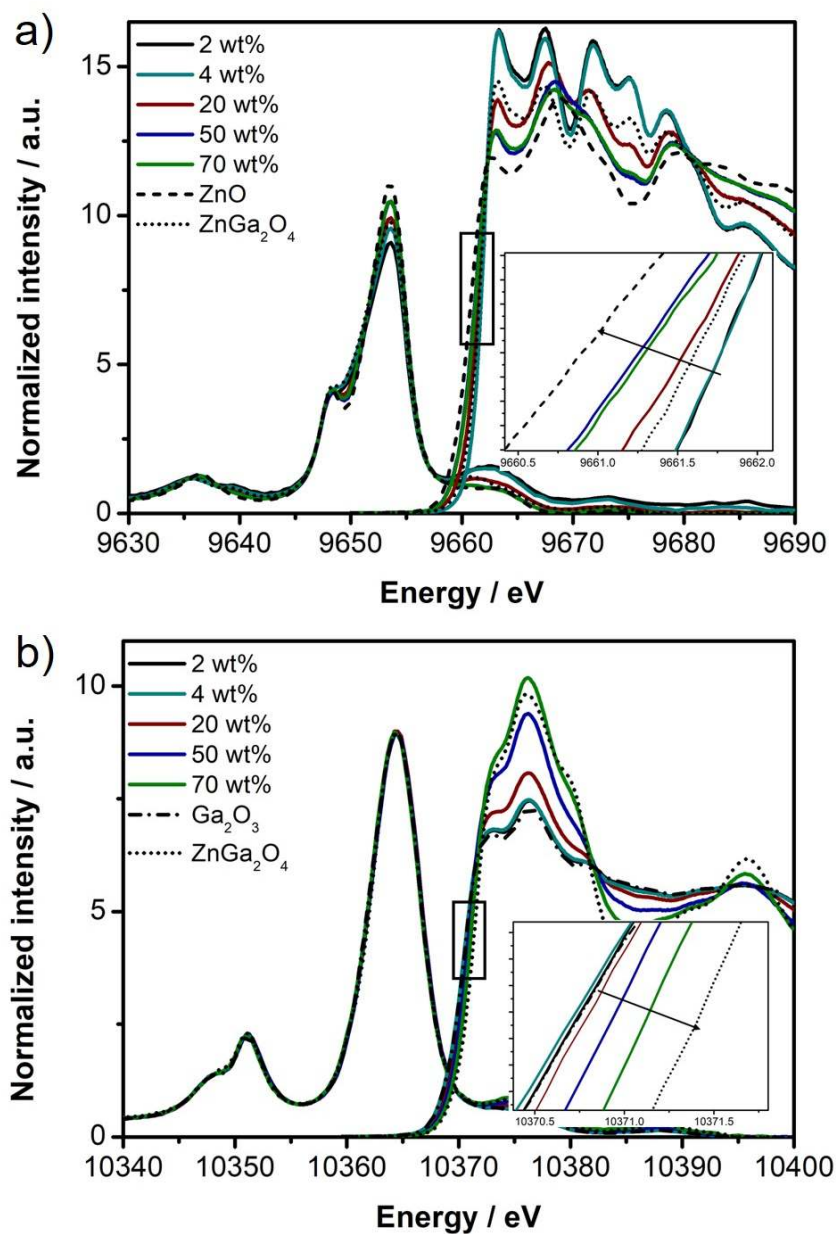
Fig. S8 XAS and VtC-XES spectra for a) Zn K-edge and b) Ga K-edge. Pure $ZnGa_2O_4$ (dotted line), ZnO (dashed line), and Ga_2O_3 (dot-dashed line). Spectral intensity was normalized to the spectral area. Inset figures show the opposite energy changes of the absorption edge.
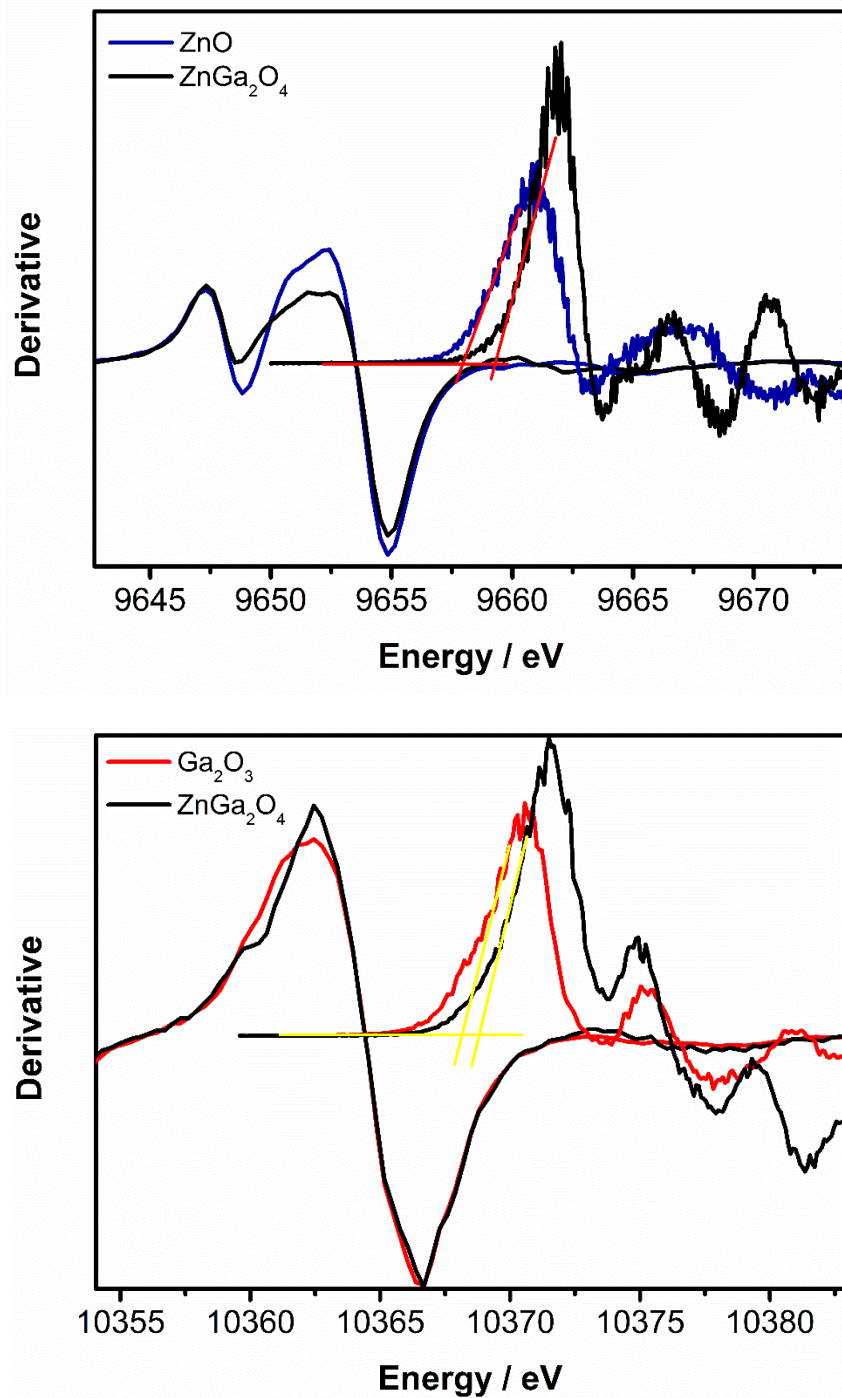
Fig. S9 First derivative of XAS and VtC-XES spectra for Zn K-edge (top) and Ga K-edge (bottom). Red and yellow lines are positioned at the intersection between baseline at 0 intensity and the slope of the first derivative of XAS, and the intersection from the baseline for XAS and XES was used to calculate the difference between the XAS and XES spectra.
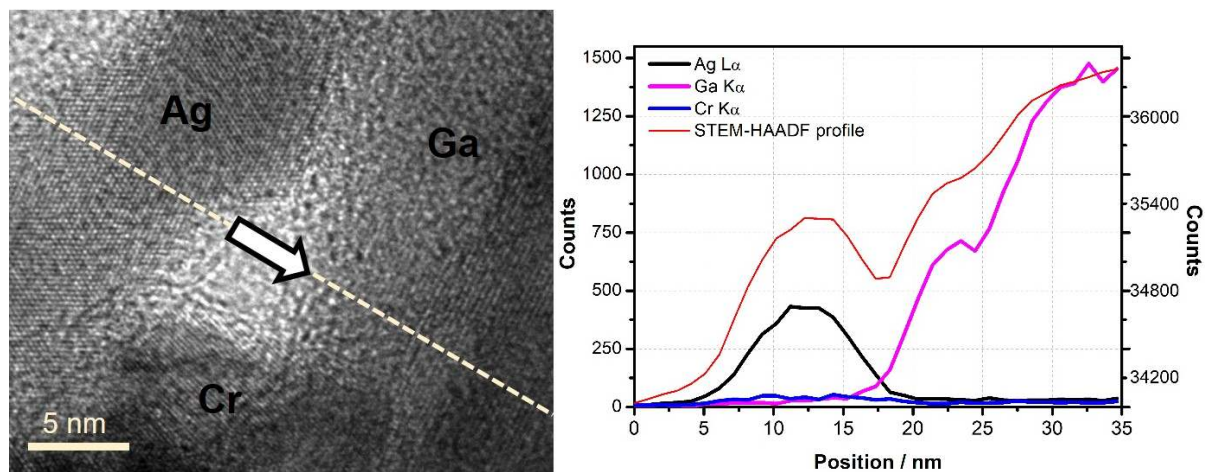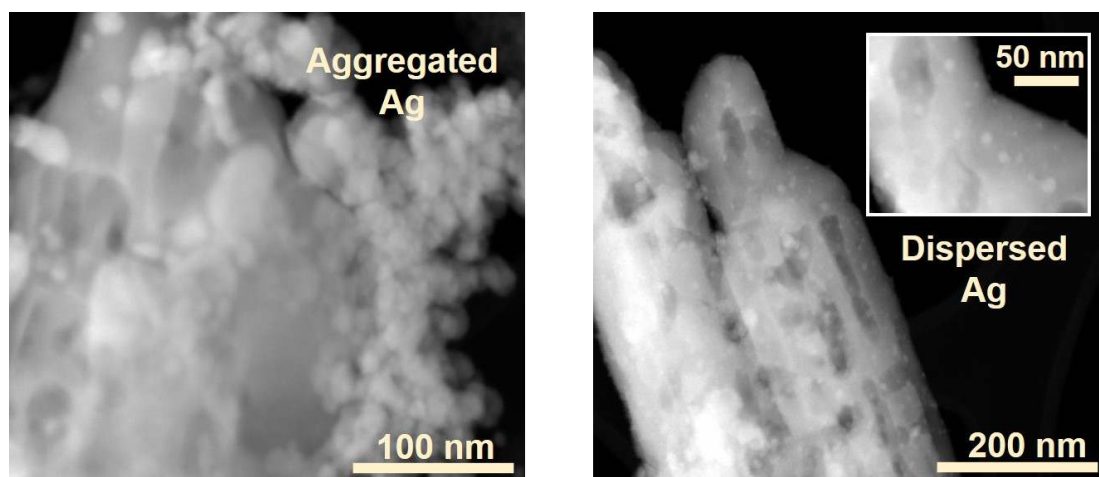
Fig. S10 STEM-HAADF image of Rh-Cr/4 wt% Zn-Ga$_2$O$_3$, and elemental profiles over the diagonal for Ag (black), Cr (blue), and Ga (pink). Rh was not detected likely due to its low content.
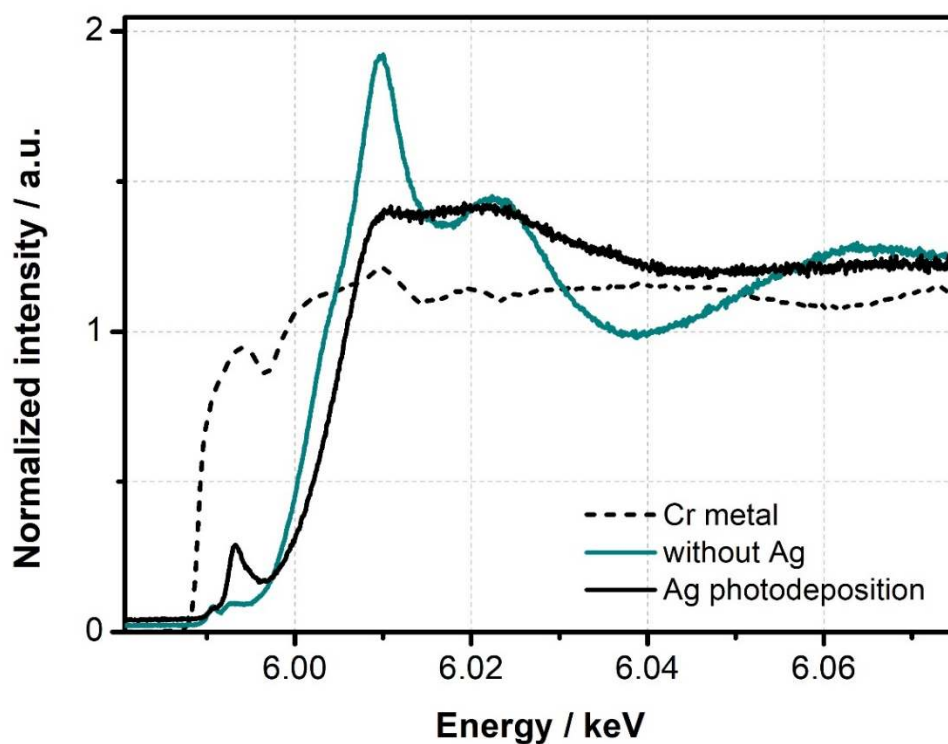

Fig. S11 XANES spectra at Cr K-edge; Cr metal (dashed line), Rh-Cr/4 wt% Zn-Ga$_2$O$_3$ (cyan), and after silver photodeposition (black).
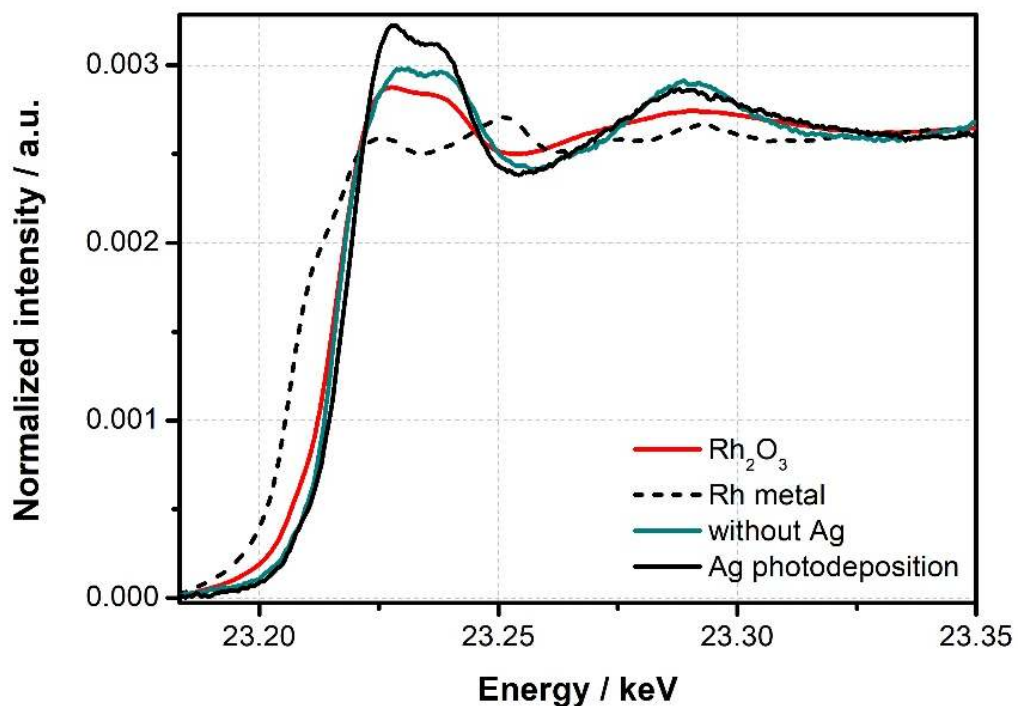
Fig. S12 XANES spectra at Rh K-edge; Rh-Cr/4 wt% Zn-Ga$_2$O$_3$ (cyan), and after silver photodeposition (black). Rh$_2$O$_3$ (red) and metallic Rh (dashed lines) were used as reference materials.

Fig. S13 STEM-HAADF images of 20 wt% Ag deposited on Rh-Cr/4wt% Zn-Ga$_2$O$_3$ after photodeposition (left) and after impregnation (right).
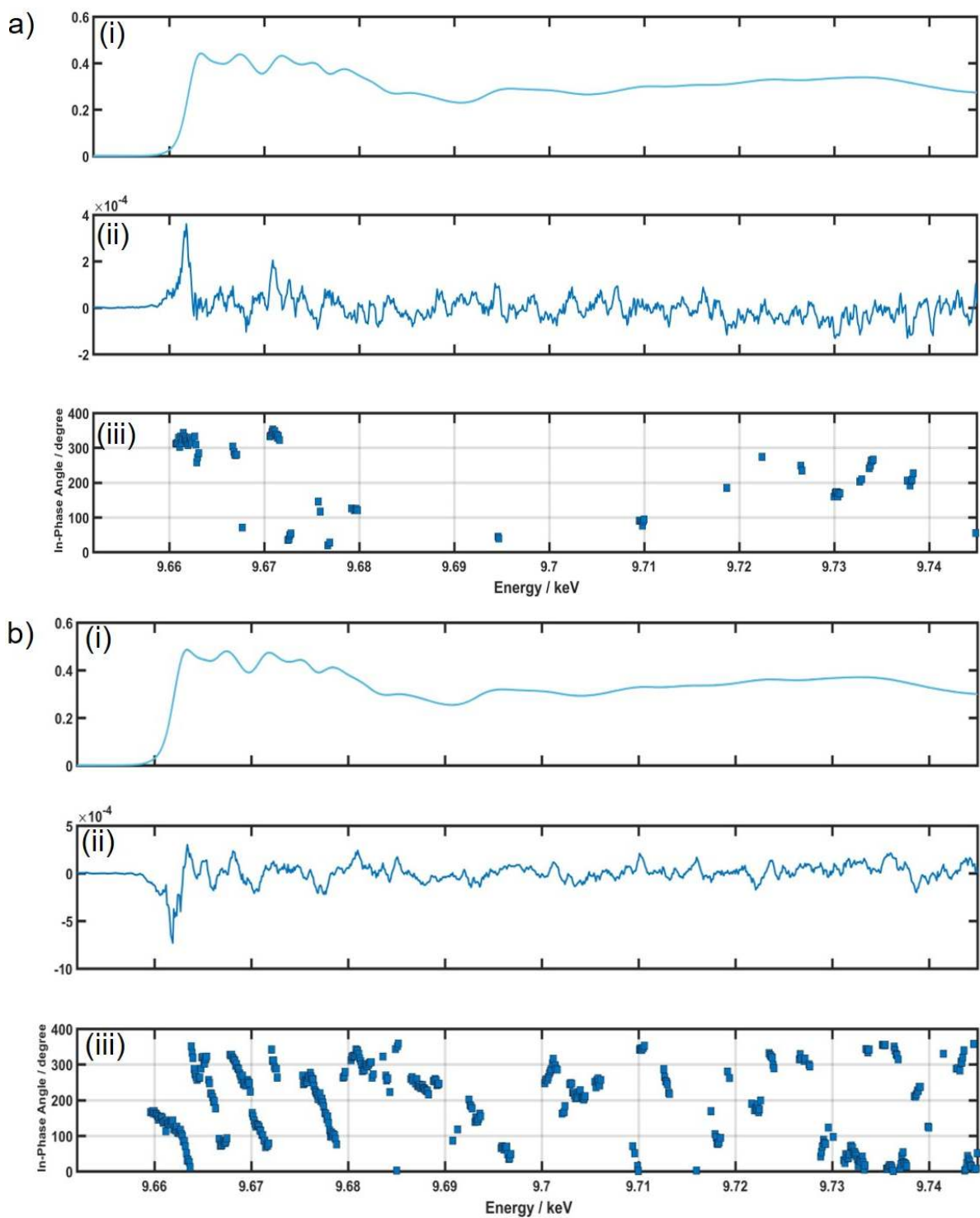
Fig. S14 Zn-Kedge HERDF-XANES phase-domain spectra and in-phase angles analysis for a) 4wt% Zn-Ga$_2$O$_3$ and b) Rh-Cr/4wt% Zn-Ga$_2$O$_3$. The amplitude threshold to plot the in-phase angles was 0.0001.

References

1. U. Bergmann, C. R. Horne, T. J. Collins, J. M. Workman and S. P. Cramer, *Chem. Phys. Lett.*, 1999, **302**, 119-124.
2. D. R. Mortensen, G. T. Seidler, J. J. Kas, N. Govind, C. P. Schwartz, S. Pemmaraju and D. G. Prendergast, *Phys. Rev. B.*, 2017, **96**, 125136.
3. R. A. Valenza, E. P. Jahrman, J. J. Kas and G. T. Seidler, *Phys. Rev. A.*, 2017, **96**, 032504.